Journal of the European Ceramic Society **15** (1995) 741–758

0955-2219/95/$9.50

0955-2219(95)00047-X

Binder Distribution in Green Ceramic Foils

G. P. van der Beek, U. Gontermann-Gehl & E. Krafczyk

Philips GmbH Forschungslaboratorien, Weisshaustrasse 2, D-52066 Aachen, Germany

(Received 7 November 1994; revised version received 10 February 1995; accepted 14 February 1995)

Abstract

Green ceramic foils with a thickness of 20 μm were tape cast on a doctor-blade machine from an aqueous dispersion of barium titanate powder, containing poly vinyl alcohol, PVA as a binder and triethylene glycol, TEG as a plasticizer. After casting, the wet foils were dried in an oven. The specific aim of this study was to characterize the binder distribution in green foils and to find parameters that affect this distribution. Mercury Intrusion Porosimetry and Nitrogen Adsorption (B.E.T.) were used as techniques to analyse the binder distribution. Experiments were carried out with foils containing either a coarse (d_{50} = 0·75 μm) or a fine barium titanate powder (d_{50} = 0·2 μm). The moment in the drying process of foils, that the binder gets fixed in the ceramic structure determines the binder distribution in green foils. The earlier the PVA fixation process takes place, the more homogeneous is the binder distribution. The plasticizer triethylene glycol (TEG) promotes fixation of PVA by a gelation process. More TEG in the slip leads to a more homogeneous binder distribution in foils. In the case of a low TEG amount, small pores are preferentially filled with binder over large ones and the lower side of foils is enriched with binder. Less hydrolysed PVA types are less susceptible to gelation with TEG, resulting in a more heterogeneous binder distribution.

1 Introduction

Thin green ceramic foils are used for the preparation of several laminated components, e.g. ceramic multilayer capacitors (CMCs)[1–3] and multilayer actuators (CMAs),[4] solid oxide fuel cells (SOFC),[5] heat exchangers,[6] ceramic superconducting elements[7] and laminated composites.[8]

Green ceramic foils consist of inorganic particles, organic substances (binder, plasticizer, dispersants, etc.), air (porosity) and moisture or organic solvent rests. The binder, which is a polymeric substance, has an adhesive function for the ceramic particles within green tapes. The binder is present during a large part of the whole processing route for ceramic components. In most cases, ceramic components are built and shaped in the green state. After that, the binder is burnt out and finally the components are sintered. The constitution and distribution of the binder within green foils influence or determine foil properties that are important for the processing of laminated ceramic components: mechanical characteristics,[9] stress sensitivity, lamination behaviour, porosity and pore sizes. The binder distribution may have a large effect on the mass and heat transfer resistance during thermolysis of green components.[10] These parameters are of crucial importance to prevent crack and defect formation. The amount of binder and the binder distribution in green foils may also affect the porosity in sintered products. Porosity in green bodies can be reduced by pressing; porosity after binder burn-out can only disappear by the sintering procedure. A high local binder content in the pressed green state leaves such a high porosity after binder removal that it cannot be sintered any more to a dense ceramic. Considering all the effects described above, the binder distribution in green foils may have a significant impact on the structural integrity of laminated green components and, eventually, on that of sintered ones as well.[11,12]

The specific aim of this study is to characterize the binder distribution in foils and to determine parameters that affect this distribution. The techniques used for this purpose are Nitrogen Adsorption (B.E.T.) and Mercury Intrusion Porosimetry.

To investigate the binder distribution, as a function of particle size (or pore size), we have analysed foils made from both coarse and fine powders. As a powder system we have taken barium titanate, which is an important material for dielectric layers.[13,14] The influences of the binder concentration, the binder type and the plasticizer content in the slip, on the binder distribution in foils have also been studied. Apart from the materials, the processing conditions (i.e. drying procedure) affect the binder distribution as well.

We will start this paper with a brief description of the drying mechanism of ceramic foils and discern the important parameters for drying. This description appears to be helpful for the interpretation of the results obtained in this study.

2 Theory of Drying

A number of studies on drying of ceramic bodies have been issued over the last few years.[15-21] An excellent paper on this issue has been written by Scherer.[17]

Several stages can be distinguished during drying of ceramic bodies. The drying mechanism, the rate-controlling factors, the stresses that may develop and the dimension changes may all be different in these stages of drying.[17-19] Each stage depends, in a particular way, upon external factors (temperature, air flow and ambient vapour pressure) and on internal factors (such as body geometry, particle packing, pore sizes). For a good controlled drying procedure, the drying conditions have to be set separately for each stage.

The first drying stage is called the *constant rate period* (CRP). Under constant external conditions, the rate of evaporation per unit surface area is independent of time and moisture content in the drying body. During the CRP, the shrinkage of the drying body is equal to the volume of liquid evaporated. The meniscus remains at the exterior surface.

The drying rate during this stage depends upon the external conditions such as ambient vapour pressure, temperature, draught and geometry of the system. In the constant rate period, the evaporation process is by definition the rate-limiting step and not the liquid transport in the green body. Evaporation is an endothermal process and has, therefore, a cooling effect. A reduced temperature upon evaporation leads to a lowering of the drying rate. This feedback process equilibrates when the drying surfaces reach the so-called *wet bulb* temperature. Hence, the drying temperature of water-based ceramic foils is determined by the humidity, the ambient temperature and the air flow.

Liquid from the interior of the green body is transferred to the evaporation surface by flow due to pressure gradients (capillary pressure) as well as by diffusion due to concentration gradients. The flow flux is the most important one in this stage.

The constant rate period ends at the so-called *critical point* where shrinkage virtually stops. At this point, the ceramic structure has been built and further drying occurs by replacing liquid in the ceramic network by air.

A phenomenon often observed during drying of ceramic tapes is the so-called *skin effect*. In such a case, the evaporation process is so fast that the concentration of binder at the surface becomes very high because the diffusion rate is too small. The binder may then precipitate or gelate to an impermeable layer which hinders the transport of the underlying liquid to the evaporation surface. The drying rate may then reduce drastically and the constant rate period is ended by definition. Skin-forming can be prevented by lowering the evaporation rate and/or increasing the diffusion flux. A reduction of the ambient temperature decreases the evaporation rate but also decreases the diffusion flux and is therefore not very effective to counteract binder segregation. Increasing the humidity and/or reducing the air flow lowers the evaporation rate. The diffusion rate may eventually be enlarged because the wet bulb temperature increases due to a lowered evaporation rate. Hence, to overcome the skin effect it is much more effective to reduce the difference between the ambient and equilibrium vapour pressures than to lower the ambient temperature. The skin-forming effect becomes less important for thinner foils because the diffusion distances are smaller.[20]

After the critical point the second drying stage sets in. This stage is called the *first falling rate period* (FRP1). The vapour/liquid interface recedes into the green body and the drying surface may begin to lose its translucency. The drying rate decreases and the temperature of the surface rises above the wet bulb temperature during this stage. Although the meniscus retreats into the green body, most of the evaporation still occurs at the exterior surface due to the fact that the liquid in the pores near the surface is in a funicular condition (i.e. continuous thin liquid pathways along the flow is still possible). Therefore, the temperature of the surface remains under the ambient temperature and the drying rate is still sensitive to external factors as temperature and vapour pressure. The liquid flux from the interior to the surface becomes, however, more and more rate-controlling. At the same time, some liquid evaporates in the unsaturated pores and the vapour is transported by diffusion.

The drying front becomes irregular in instances where different pore sizes are present. At the critical point, the radii of the menisci in different pores are equal and therefore the capillary pressures are equal. Upon further drying, the meniscus radii of the small pores get smaller than those of the large pores. This leads to different capillary pressures in large and small pores. As a consequence, liquid flows from large pores to smaller ones. Hence, large pores are emptied before the small ones.

In the last drying stage, the *second falling rate period* (FRP2), the flux of the liquid is very slow.

Eventually, the flow to the surface stops, the liquid is isolated in pockets (mainly the small pores) and can only be removed from the green body by vapour diffusion. This diffusion process controls the drying rate, which is therefore less dependent upon external factors, and the evaporation process takes place completely inside the body. The temperature of the surface approaches the ambient temperature.

3 Preparation of Foils

Both ceramic foils containing coarse barium titanate powder and foils containing fine barium titanate powder were made and analysed in this study. These foils were prepared by tape casting on a doctor-blade machine.[22-24] The conducted procedure was as follows. Dielectric powder was dispersed into water with the help of a dispersant. The amount of dispersant added was equal to that needed for a minimum value of the yield value and of the viscosity. Of course, more dispersant per weight unit of solid material had to be added to the fine barium titanate powder because of the larger specific surface area (due to smaller particles). The obtained dispersion, which is called a slurry, is then de-agglomerated by ultrasonification (15 min in a US bath of 200/400W) and milling (Attritor-mill filled with 2 mm ZrO_2 balls at 500 rpm; 20 min milling for the fine powder and 40 min for the coarse powder sample). The average diameter of the coarse barium titanate particles in the slurry was about 0·75 μm (= d_{50} as measured by X-ray absorption in a sedimentation experiment using the Micromerites Sedigraph 5000D). This value was equal to 0·2 μm for the fine barium titanate sample. After sieving the slurry, the constituents listed below are added and the suspension is then called a *slip*.

- The binder poly vinyl alcohol, PVA. The rheological behaviour of the slip, which is important for the casting process, may be adjusted by the amount and/or type of binder. When the solvent evaporates after tape casting, the ceramic particles within the foil are held together by the binder. In our study, we used different PVA samples, which are given in Table 1.
- The plasticizer triethylene glycol, TEG. In general, the plasticizer structurally expands the binder and improves the distribution of the binder in the slip. The flexibility of green foils may be increased by the addition of a plasticizer, which lowers the glass transition point, T_g of the binder.

Table 1. Poly vinyl alcohol samples used in this study

PVA sample	$\overline{M_w}$ *(g mol^{-1})*	*hydrolysis ratio*[a] *(mol%)*
PVA 31-88	31 000	87·7 ± 1·0
PVA 27-98	27 000	98·4 ± 0·4
PVA 125-98	125 000	98·4 ± 0·4
PVA 205-88	205 000	87·7 ± 1·0

[a]Poly vinyl alcohol is made from poly vinyl acetate. The hydrolysis ratio is the percentage of acetate groups hydrolysed to alcohol groups.

- Small amounts of an anti-foam agent (to counteract foam formation during mixing), a wetting agent (to have a good wetting behaviour of the slip on the tape casting carrier) and a release agent (to release the green foil from the carrier).

Concentrations of PVA and TEG are always expressed in wt% relative to the solid material throughout this study. After all these additions, the resulting slip was finally degassed before tape casting took place to prevent holes in the foil caused by enclosed air bubbles. Care was taken to prepare the slurry and slip always in the same way in order to be able to compare the foil properties properly.

In this study, 20 μm green foils (unless otherwise stated) were cast from a slip with the help of a doctor-blade machine and subsequently dried in an oven (without air circulation). Because the drying procedure may affect the foil properties, results presented in this study are all based on foils which were dried in the same way, i.e., at 60°C for 30 min. After drying, the foils were carefully released from the substrate.

The binder content and plasticizer concentration in slips are varied in this study. Changes in these concentrations were always compensated for by the amount of water added. In this way, the solid content of all slips could be kept the same (i.e. 45·6 wt%). Variation in the solid content leads to a different drying procedure, which may influence the foil characteristics.

4 Measuring Methods

Both Nitrogen Adsorption (B.E.T.) and Mercury Intrusion Porosimetry may yield information about the binder distribution within a green ceramic foil. Neither of these methods gives, however, a real binder concentration profile over the thickness of the foil.

4.1 B.E.T. nitrogen adsorption

Gas adsorption onto solid phases was first

described by Brunauer, Emmet and Teller (B.E.T.). They derived the following adsorption isotherm:

$$\frac{V}{V_m} = \frac{C(P/P_0)}{[1-(P/P_0)]\,[1 + (C-1)\,(P/P_0)]}$$

where V_m is the volume of one adsorbed monolayer, P is the vapour pressure of the adsorbate and P_0 is the saturated vapour pressure at the temperature of adsorption. The constant C is a measure for the affinity of the adsorbate molecules for the surface. A large C value indicates a strong interaction of the adsorbing molecules to the substrate (so-called 'high energy' surface). Hence, the form of the isotherm depends upon the substrate material. Isotherms with C-values between 1 and 100 are quite usual. Inorganic oxide surfaces have a high C-value most of the time.

The specific surface area (S) can be calculated from the V_m value using the molecular dimension of the adsorbate molecules. Because V_m stays explicitly in the equation of the adsorption isotherm, S can be determined from the experimental adsorption data.

Adsorption hysteresis is frequently found for gas adsorption onto porous media. This hysteresis effect can be explained by capillary condensation. Small pores will be filled with adsorbate at a high vapour pressure, forming a concave adsorbate meniscus. According to Kelvin's law, the evaporation from a flat liquid surface and a concave liquid surface as a function of the vapour pressure is different. Hence, the desorption isotherm will be influenced by capillary condensation. This hysteresis effect is, of course, dependent upon the size of pores. A pore size distribution can, in principle, be determined from the hysteresis effect. Obviously, only small pores (2 nm $\leq d_{pore} \leq$ 50 nm) can be detected in this way.

4.1.1 Analyses

Ceramic foils, with and without binder (after binder burn-out), as well as the ceramic powders were analysed using the ASAP 2000 B.E.T. apparatus from Micromeritics. Nitrogen gas was used as an adsorbate. Before each measurement, the sample was degassed under vacuum at 50°C for about 15 h. The surface affinity to nitrogen adsorption was determined by calculating the C-value from the adsorption isotherm. Changes in the chemical nature of the surfaces inside pores may be detected with the help of this parameter.

As already described in the previous section, small pores can be determined by the B.E.T. adsorption technique. However, we did not pay very much attention to this feature of the B.E.T technique for the following two reasons:

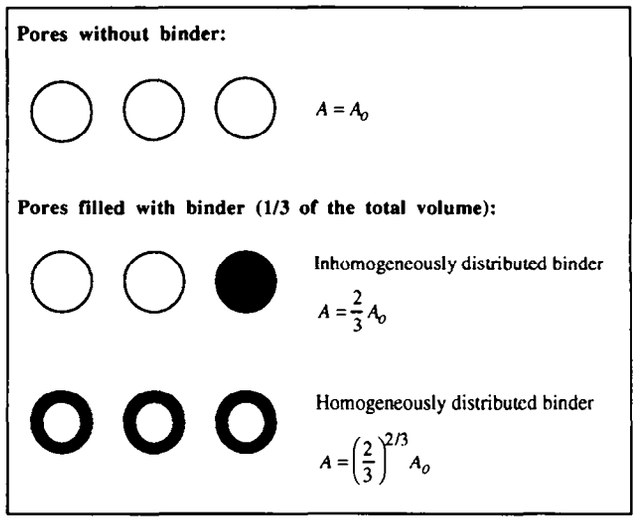

Fig. 1. Surface areas of spherical pores differently filled with binder.

(1) the pore size distribution of most of the foils goes beyond the detection limit of this technique,
(2) the pore size distribution can be measured more accurately by Mercury Intrusion Porosimetry (see next section).

The specific surface area of a green foil depends upon (i) the primary particle size, (ii) the ceramic structure, (iii) the total amount of binder and (iv) the binder distribution. An example of the correlation between the specific surface area of foils and the binder distribution is given in Fig. 1. A foil with an inhomogeneous binder distribution always has a lower surface area than a foil containing a homogeneously distributed binder.

4.1.2 Relationships between the surface area and the binder distribution in foils

Theoretical dependencies of the surface area on the total amount of binder in foils are derived in the Appendix for four special cases. These instances differ in pore geometry and/or binder distribution. The formulas belonging to these different cases are given below. The parameters used in these formulas are:

A_0 The specific surface area of a foil without binder
A The specific surface area of foils containing a certain amount of binder
P_0 The total porosity of foils without binder (not to confuse with the saturated vapour pressure in the B.E.T. adsorption isotherm)
V_i The amount of organic substances (binder, dispersant, etc.), expressed in vol.% with respect to the ceramic material.

4.1.2.1 Spherical pores filled homogeneously with binder. In this case, the added amount of binder with respect to the ceramic is assumed to affect only the radius of the pores (see Fig. 1).

$$A = A_0\left[1-\frac{1-P_0/100}{P_0}V_i\right]^{2/3} \quad (1)$$

4.1.2.2 Pores filled inhomogeneously with binder. In this instance, the amount of added binder with respect to the ceramic is assumed to affect only the number of filled and unfilled pores. This dependency is invariant of the pore geometry. The same relationship holds also for cylindrical pores that are filled from the bottom to the top (the filling height of the cylinders changes with the amount of binder).

$$A = A_0\left[1-\frac{1-P_0/100}{P_0}V_i\right] \quad (2)$$

4.1.2.3 Cylindrical pores filled homogeneously with binder. In this case, the amount of added binder with respect to the ceramic is assumed to affect only the diameter of the cylinder.

$$A = A_0\left[1-\frac{1-P_0/100}{P_0}V_i\right]^{1/2} \quad (3)$$

4.1.2.4 Small spherical pores preferentially filled with binder over large ones. The previous relationships were all based on the assumption that pores are filled equally over the size distribution. Suppose that three different pore sizes (spheres with radii of $0{\cdot}5R$, R, and $2R$) exist in a ceramic foil without binder. The number of pores, for each type, is chosen such that the volume of each class of pores is equal to one third of the total porosity. An inhomogeneous binder distribution is assumed, i.e. pores are filled one by one by the binder. Suppose that first the small pores are filled with binder, then the medium sized ones, and finally the big ones. The total surface area as a function of the amount of binder is then described by the following set of relations:

$$A = A_0\left[1-\frac{12}{7}\left(\frac{1-P_0/100}{P_0}\right)V_i\right] \quad (4a)$$

$$\text{for } 0 \le V_i \le \frac{1}{3}\frac{100P_0}{(100-P_0)}$$

$$A = A_0\left[\frac{5}{7}-\frac{6}{7}\left(\frac{1-P_0/100}{P_0}\right)V_i\right] \quad (4b)$$

$$\text{for } \frac{1}{3}\frac{100P_0}{(100-P_0)} \le V_i \le \frac{2}{3}\frac{100P_0}{(100-P_0)}$$

$$A = A_0\left[\frac{3}{7}-\frac{3}{7}\left(\frac{1-P_0/100}{P_0}\right)V_i\right] \quad (4c)$$

$$\text{for } \frac{2}{3}\frac{100P_0}{(100-P_0)} \le V_i \le \frac{100P_0}{(100-P_0)}$$

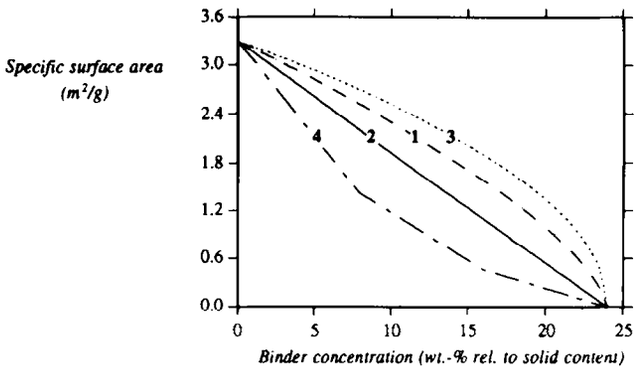

Fig. 2. Theoretical relations between the specific surface area and the amount of added binder relative to the ceramic for foils containing the coarse barium titanate. The numbers correspond to the different cases described above. The following parameters were used for the calculations: P_0 = 55%, A_0 = 3·3 $m^2.g^{-1}$, ρ_{binder} = 1·2 $g.cm^{-3}$, $\rho_{ceramics}$ = 5·9 $g.cm^{-3}$.

All the dependencies given above are visualised by the curves given in Fig. 2. As can be seen in this figure, a high surface area corresponds to a homogeneous binder distribution (cases 1 and 3). Surface area values lower than those given by case 2 can, in principle, only occur if small pores are filled preferentially over large ones.

In order to be able to compare binder distributions of different systems by measuring the specific surface area, we have defined a so-called *binder distribution index*, X:

$$X = \frac{A - A_0\left[1-\frac{1-P_0/100}{P_0}V_i\right]}{A_0\left[1-\frac{1-P_0/100}{P_0}V_i\right]^{1/2} - A_0\left[1-\frac{1-P_0/100}{P_0}V_i\right]} \quad (5)$$

This index is 0 for specific surface areas corresponding to line 2 in Fig. 2, and 1 for values corresponding to curve 3. Hence, the larger the index X, the more homogeneously is the binder distributed. We have to note, however, that high X-values can, in principle, also be due to the fact that large pores are preferentially filled with binder over small ones. In practice, this will rarely occur because large pores are emptied first during drying (by capillary action). On the other hand, negative X values are more probable because of the tendency that small pores are preferentially filled with binder.

4.2 Mercury intrusion porosimetry

The principle of Mercury Intrusion Porosimetry is based on the fact that mercury behaves as a non-wetting liquid towards most substances. Consequently, it does not intrude into the pores of these substances without applying pressure. Mercury porosimetry measurements are conducted by measuring a series of pressures with corresponding

volumes of mercury intruded into the porous body. The pore radius (r) can be calculated from the applied pressure (ΔP), the surface tension of mercury (γ_{LV}) and an assumed wetting angle (θ), using the Washburn equation:

$$\Delta P = \frac{2\gamma_{LV}\cos\theta}{r} \quad (6)$$

The total amount of pores with a certain radius is simply calculated from the volume of intruded mercury at the pressure corresponding to that pore size.[25–28] The total pore volume can be determined if all pores have been filled at the maximum pressure of the equipment. The porosity can then be calculated if the total volume of the sample is known.

A few things should be taken care of using Mercury Intrusion Porosimetry. These items can be summarized as follows:

1. Mercury Intrusion Porosimetry often displays hysteresis phenomena. The pressure-volume relationship is different for penetration and retraction of the mercury. A certain amount of mercury may remain in the porous medium after complete reduction in the pressure. Two causes are mainly responsible for this phenomenon:
   - — The advancing contact angle is often different from the receding one. Different penetration and retraction curves will then be obtained.
   - — Structural hysteresis refers to the presence of the so-called *ink-bottle* pores (i.e. pores with a small opening). During penetration, one big ink-bottle pore is measured as a number of small ones with radii equal to that of the opening of the big pore. In general, the effect of structural hysteresis will be less if the porosity is higher. However, the details of this phenomenon will depend upon the particular geometry of the pore space.
2. If a number of hysteresis loops are recorded, the first penetration curve is different from subsequent ones. A difference in contact angle for a fresh surface and a surface that has already been in contact with mercury may be the reason for this phenomenon.
3. For easily deformable samples, geometrical and pore size changes may occur by the applied pressure (compression).

Assuming that the pores are series of cylinders of different diameters, the surface area can be calculated by integrating the volume–diameter curve. Specific surface areas determined in this way are, in most cases, higher than those obtained from sorption isotherms (B.E.T.) due to the presence of *ink-bottle* pores. We do not use this feature of Mercury Intrusion Porosimetry because the determination of the specific surface area by this technique is less reliable than that of B.E.T. measurements.[25, 28]

4.2.1 Measurements

The measurements were conducted with a Porosimeter 2000 from Fa. Carlo Erba Instruments. Samples that were both analysed by nitrogen sorption and porosimetry were first used for the specific surface area measurement and afterwards put into the porosimeter vessel. Samples of about 15 cm^3 were evacuated for about 1 h before immersing in mercury at a low pressure (0·1 MPa). The Hg-pressure was increased step-wise. The pressure was enlarged only if the volume of intruded mercury had become constant. After a complete reduction in the pressure, a second run was started. All measurements were carried out at room temperature.

We used the following values for the parameters needed to calculate the pore sizes: γ_{LV} = 0·485 N m^{-1} and θ = 140°. For comparison of the porosity and pore sizes between samples of the same nature, it is not really necessary to know the exact values of these parameters. The pore size distribution is indicative of binder distribution in a foil, as can be seen in Fig. 1. Only the number of large pores is diminished for a very inhomogeneous binder distribution. The pore sizes remain unchanged in such a situation. In the case of a homogeneously distributed binder, the pore sizes get smaller with respect to pores in foils without binder.

5 Results

Results from measurements, as mentioned above, are described in this section. Firstly, analyses of the ceramic powders used to process the foils in this study are given. Then the results of foils released from binder are reported, and lastly the characterization of green foils is described. The interpretation and discussion of the results is partly done in a separate paragraph (Section 6).

5.1 Powders

For a correct analysis of green ceramic tapes, characterization of the powders, from which these foils were made, is needed. Porosity measurements were only possible when powders were pressed (or centrifuged) to a coherent pill. The results of the powder analyses are summarized in Table 2.

Table 2. Powder analyses

System	*C*	*B.E.T. surface* ($m^2 g^{-1}$)	*Porosity* (%)	d_{50} *pore size (nm)*
Coarse barium titanate #1:				
Without pre-treatment	103·3	2·91		
Isostatically pressed at 320 MPa	97·7	3·24		
Slurry, 40 min milled, dried	78·5	3·32		
Slurry, 40 min milled, centrifuged	62·3	3·20	37·6	181
Slurry, 40 min milled, dried, pressed at 320 MPa	64·0	3·40	36·1	152
Coarse barium titanate #2:				
Without pre-treatment	108·6	2·87		
Powder-PVA granules	40·4	1·19		
50 wt% powder-PVA granules + 50 wt% powder	76·7	2·14		
Fine barium titanate:				
Without pre-treatment	106·1	9·09		
Isostatically pressed at 3·2 kbar	113·3	9·83	37·9	61
Slurry, 20 min milled, dried	78·7	9·34		
Slurry, 20 min milled, centrifuged	78·6	9·36	38·9	56
Slurry, 20 min milled, dried, pressed at 320 MPa	75·4	9·27	37·6	50
PVA 125-98:				
Crushed granules, dried at 50°C	20·1	–	–	–

5.1.1 B.E.T. analyses

The specific surface areas of the fine and coarse powders without any special treatment are equal to 9·1 $m^2 g^{-1}$ and 2·9 $m^2 g^{-1}$, respectively. No significant difference was found between two different batches of the coarse sample (batch #1 and #2 in Table 2). As expected, the specific surface area of the fine powder sample is much higher than that of the coarse powder due to the smaller particles.

As can be seen in Table 2, the *C*-values of the powders without any pre-treatment are equal to about 105, indicating 'high energy' surfaces. Just isostatically pressing the powders does not change the B.E.T. values very much. The specific surface area seems to increase a little upon this treatment.

We also analysed the powders from the slurries made as described in Section 3. The powders were separated from the slurries either by simply drying or by centrifugation and subsequently drying the centrifuged cake. The specific surface areas of the powders from the slurries are slightly higher than those of the ones without any pre-treatment because of the milling procedure used for the preparation of slurries. This effect is not very large because the surface area of particle aggregates is not very different from that of separated particles. The *C*-values of the slurry powders are all about 75, which is significantly lower than those found for untreated powders. This effect is caused by the adsorption of the dispersant onto the particle surfaces. The chemical nature of the surface, and hence the affinity to nitrogen adsorption, have been changed by this adsorption process.

In order to investigate the influence of the poly vinyl alcohol on the *C*-parameter, we dispersed coarse powder (batch #2) into a PVA solution. The binder concentration with respect to the ceramic material was of the same order as that used in slips (i.e. 8 wt%). Thin films of this dispersion were dried in a oven at 60°C. The product obtained in this way was analysed by the B.E.T. technique. The *C*-value of these powder-PVA granules was equal to 40·4. A mixture of 50 wt% of this product and 50 wt% of untreated powder gave a *C*-value of 76·7 (mixing was done in the dry state). Hence, the B.E.T. technique is sensitive to the degree of powder particle coating with PVA. This effect is graphically shown in Fig. 3.

Finally, we have measured the *C*-value of pure PVA 125-98. This turned out to be about 20, i.e.

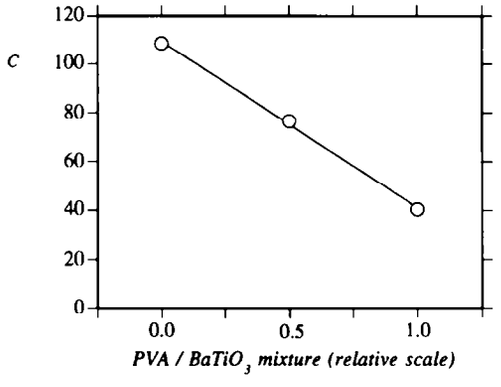

Fig. 3. Surface affinity to nitrogen adsorption (*C*-value) of coarse $BaTiO_3$/PVA mixtures as a function of the PVA concentration: 0.0, pure $BaTiO_3$ powder; 1.0, PVA/$BaTiO_3$ granules (8·0 wt.% PVA with respect to barium titanate); 0·5, pure $BaTiO_3$ powder mixed with the same PVA/$BaTiO_3$ granules as in 1·0 in a weight ratio of 1:1.

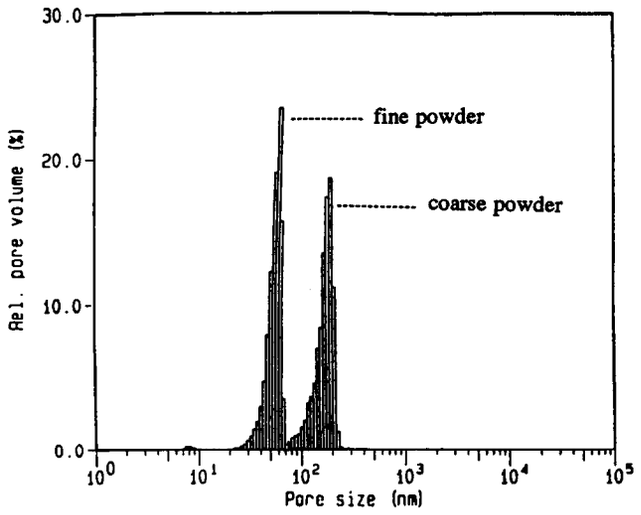

Fig. 4. Pore size diagrams of pills centrifuged from slurries containing the two grades of powder.

the lowest value found so far. Apparently, the nature of the ceramic powder in the dried PVA/$BaTiO_3$ mixture (C = 40) was not fully masked by PVA. The powder particles were, probably, not completely or sufficiently wetted (coated) by the PVA in the dispersion.

5.1.2 Porosimetry

The pore size distributions of powders centrifuged from slurries to a coherent tablet are given in Fig. 4. As can be seen in this figure, the pore sizes for the finer powder batch (d_{50} pore size ≈ 60 nm) are much smaller than for the coarser sample (d_{50} pore size ≈ 190 nm).* A measure of the particle packing is the d_{50} pore size divided by the d_{50} particle size. These numbers lay between 0·20 and 0·30 for both powders. Values of about 0·14 (= 1/7) are found for an ideally closed packed system of monodisperse particles. Hence, both powder pills have the same fairly close particle packing. This is supported by the total porosity measurements. The total porosity for the coarse powder system and the fine powder system are the same, i.e about 37%. For comparison, the porosity of a closed packed system of monodisperse particles is equal to 26%. Apparently, the slurries did not contain large aggregates.

5.2 Foils

A green foil can be conceptualized as a ceramic structure containing organic material. First, the ceramic structure of foils will be discussed. Paragraph 5.2.2. deals with the distribution of organic material within the ceramic structure.

5.2.1 Foils released from organic material

Green foils were released from the organic substances by heating in air at 550°C for 1 h. Both foils consisting of coarse and fine powder were analysed. The influences on the ceramic structure of the binder type, binder concentration and the amount of plasticizer added to the slip have been studied. All results of these measurements are summarized in Table 3.

The C-values and the specific surface areas measured for these burned foils come close to those found for the untreated powders in Table 2.

*The d_{50} value is the pore size at which half of the total porosity is filled with mercury.

Table 3. Analyses of foils released from organic material

PVA type and concentration present in the foils before binder removal	*TEG conc. in the slip (wt%)*	*B.E.T. results*		*Porosity (%)*	*d_{50} pore size (nm)*
		C	*S ($m^2 g^{-1}$)*		
Coarse barium titanate:					
6·5 wt% PVA 205-88	0	83	3·46	55·9	380
6·5 wt% PVA 125-98	0	109	3·63	53·1	364
6·5 wt% PVA 205-88	2·6	96	3·34	55·7	372
6·5 wt% PVA 125-98	2·6	108	3·40	56·5	390
8 wt% PVA 205-88	0	140	3·30	53·6	457
8 wt% PVA 125-98	0	86	3·25	56·9	466
6·5 wt% PVA 205-88 + 1·5 wt% PVA 27-98	0	88	3·38	–	...
6·5 wt% PVA 125-98 + 1·5 wt% PVA 31-88	0	138	3·35	55·7	417
6·5 wt% PVA 125-98 + 1·5 wt% PVA 27-98	0	119	3·33	54·0	463
8 wt% PVA 205-88	3·2	107	2·99	55·0	383
8 wt% PVA 125-98	3·2	118	3·32	52·0	390
6·5 wt% PVA 205-88 + 1·5 wt% PVA 27-98	3·2	108	2·92	55·1	393
6·5 wt% PVA 125-98 + 1·5 wt% PVA 27-98	3·2	117	3·27	56·1	439
12 wt% PVA 125-98	1·6	87	3·13	52·2	408
Fine barium titanate:					
6·5 wt% PVA 20/98	3·2	107	9·27	55·1	136
8 wt% PVA 20/98	1·6	113	8·97	54·0	132
8 wt% PVA 20/98	3·2	109	8·48	55·3	147

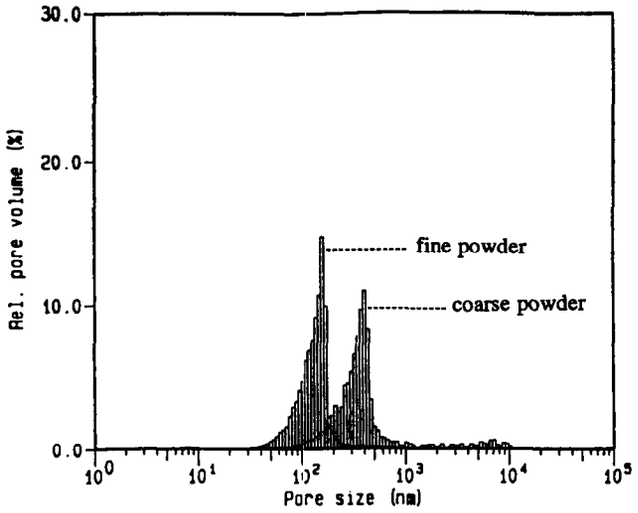

Fig. 5. Pore size diagrams of foils without binder. One foil consists of the fine powder, the other one of the coarse powder.

However, the spread in the *C*-values is quite large. Apparently, the powder surface is not left in a completely reproducible condition after the removal of the organic species. This can possibly be caused by the presence of carbonaceous residues.

As can be seen in Table 3, there is no significant change in either the total porosity or the pore sizes as a function of the slip parameters mentioned above. Hence, the ceramic structure is independent of the PVA type, the PVA concentration, and the TEG concentration within the ranges used in this study. The pore size distributions of a coarse powder and a fine powder foil without organic material are given in Fig. 5. The d_{50} pore sizes in burned foils containing either coarse or fine ceramic powder are 410 nm and 140 nm, respectively.

Both foil types without binder exhibit the same porosity (i.e. about 55%). The average values of the ratio of the d_{50} pore size over the d_{50} particle diameter are equal to 0·54 and 0·69 for the coarse and fine powder foils, respectively. Although this ratio is somewhat larger for fine powder foils than for coarse powder foils, it is questionable whether or not this difference is significant.

Both the porosity and the ratio of pore size to particle size show, however, that the powder particles are less well packed in the foils than in the centrifuged pills. This indicates that the colloidal system in the slip, during the settlement of the powder particles, was most probably not stable. This may be caused by depletion flocculation of particles in the slip due to the presence of the relatively high amount of polymer.

5.2.2 Binder distribution in green foils

The porosimetry and B.E.T. results for green foils, as a function of the binder system, are directly indicative of the distribution of the organic matter in the foils because the ceramic structure is not significantly affected by the constitution of the binder system (see previous section). The influences of the TEG content in the slip, and the PVA type and concentration, on the binder distribution in both coarse powder and fine powder foils are described in the following sections.

5.2.2.1 TEG concentration. Triethylene glycol is a relatively small molecular weight plasticizer which is not very compatible with PVA.[29] As a consequence, TEG can be removed quite easily from thin green foils. Foils may even lose TEG during storage. For instance, most of the TEG can be removed by putting thin green foils between sheets of paper for about 10 days (no plasticizing effect could be observed any more after such storage). The TEG diffuses out of the foils into the paper. All foils used for the experiments described in this section were stored between paper for at least 10 days. Moreover, the foils were evacuating at 50°C or 150°C in the B.E.T. apparatus before a measurement was carried out. So, we can assume that almost no TEG was present any more in the foils during the measurements. This is supported by Fig. 6, which shows porosities of foils prepared with different amounts of TEG. The lines given in

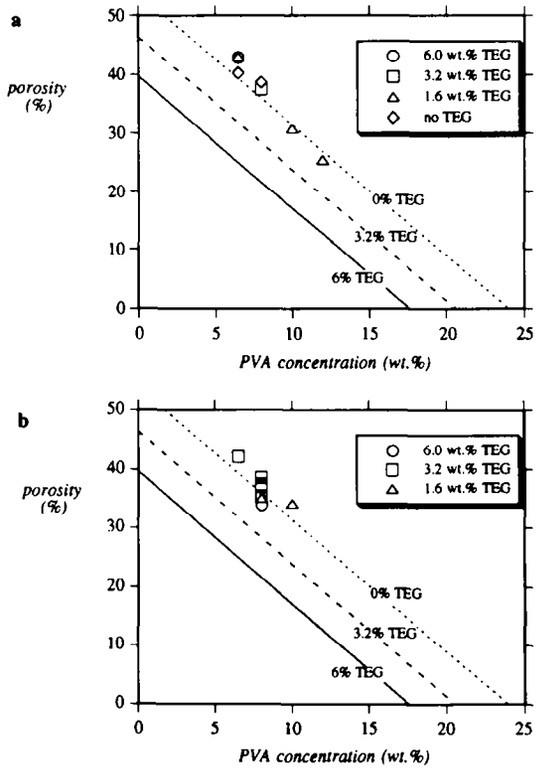

Fig. 6. The porosity of coarse particle green foils (a) and fine particle green foils (b) as a function of the PVA concentration (in wt.-% relative to the ceramic content). The given lines were calculated from the porosity of foils without binder and the densities of the organic substances, the symbols are measured values. Parameters used for the porosity calculation: P_0 = 55%, ρ_{BaTiO_3} = 5·9 g.cm^{-3}, ρ_{TEG} = 1·1 g.cm^{-3}, ρ_{PVA} = 1·2 g.cm^{-3} and 0·4 wt.% other organic substances.

this figure show porosities calculated as a function of the PVA concentration, based on a porosity of the ceramic structure of 55%. These calculations were done for different amounts of TEG present in the foils. The TEG concentrations chosen are equal to those used in several slips. A constant amount of dispersant and other substances is also taken into account (i.e. 0·4 wt% with respect to the ceramics). The measured porosities of foils are compared to calculated values. All the measured porosities (both for the fine and the coarse foils) fall around the line calculated for the case where no TEG is present in the foils. This means that TEG has indeed left the foils and that a direct influence of TEG on the pore size distribution and the specific surface area of foils can be neglected.

Pore size distributions of foils made from slips containing different amounts of TEG are given in Fig. 7. The same trend can be observed for both coarse and fine particle foils. The pore size distribution changes as a function of TEG concentration in the slip. Hence, TEG influences indirectly the binder distribution in foils. In the case where no TEG was used, a fairly thin peak could be found at the same position as the one observed for foils released from binder (see Fig. 5). In the presence of TEG, a second peak at a smaller pore size appears. Sometimes a third very small peak can be observed, especially for coarse foils (position around 1 μm). This peak is, however, independent of the TEG concentration. Whether this peak corresponds to pore sizes with these dimensions or not is doubtful.

We have to note that all pore size diagrams presented in this paper are volume distributions. Hence, one big pore has a much larger contribution to the peak area than one small pore. For a number distribution, the amount of large pores would be much smaller and that of the small pores much larger.

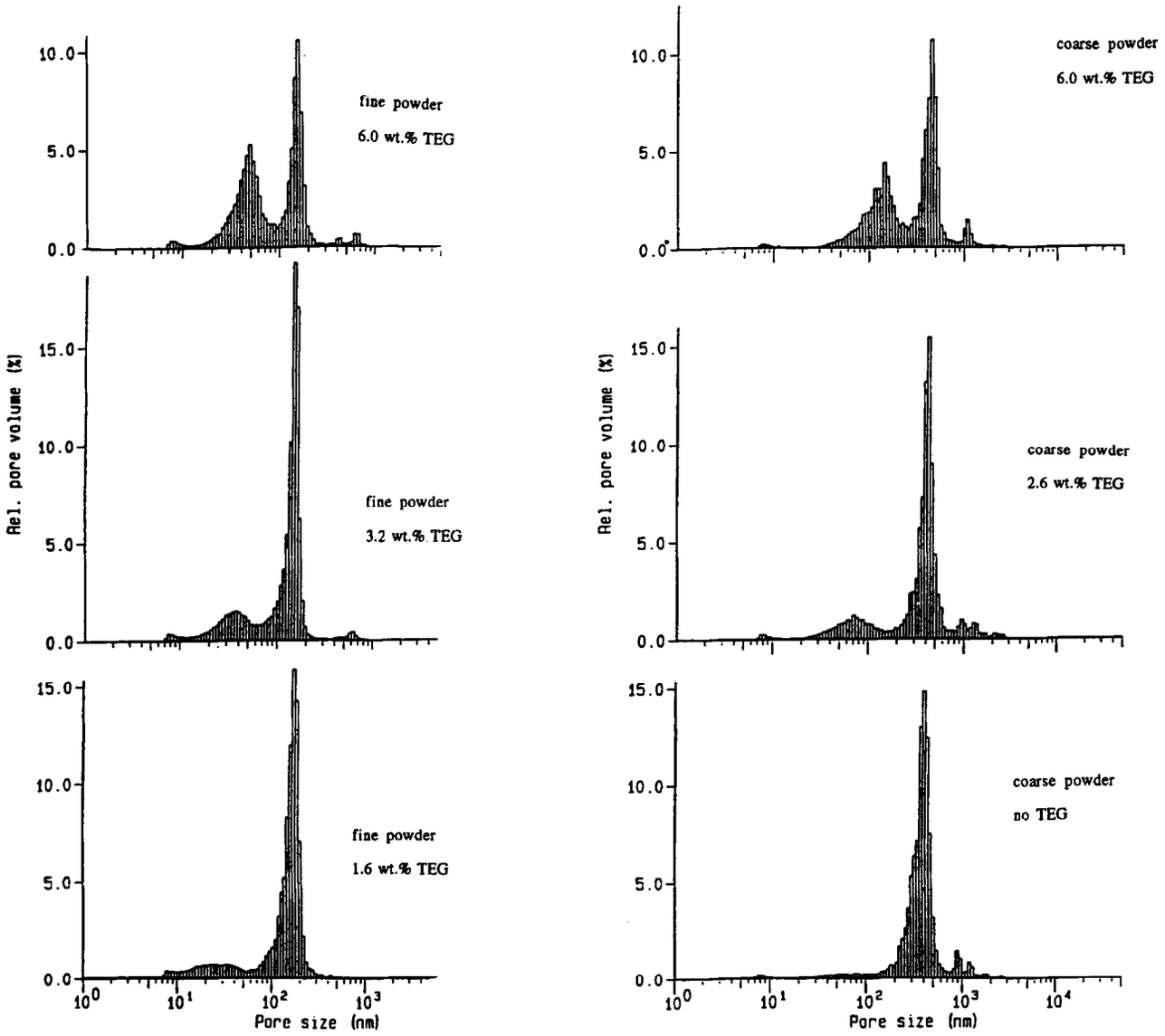

Fig. 7. Pore size distributions of coarse and fine particle green foils as a function of the amount of TEG used in the slip. The TEG concentrations are indicated in the figure (expressed in weight ratio). The PVA 125-98 concentrations were 6·5 wt.-% and 8·0 wt.-% with respect to the solid content for the coarse and fine particle foils, respectively.

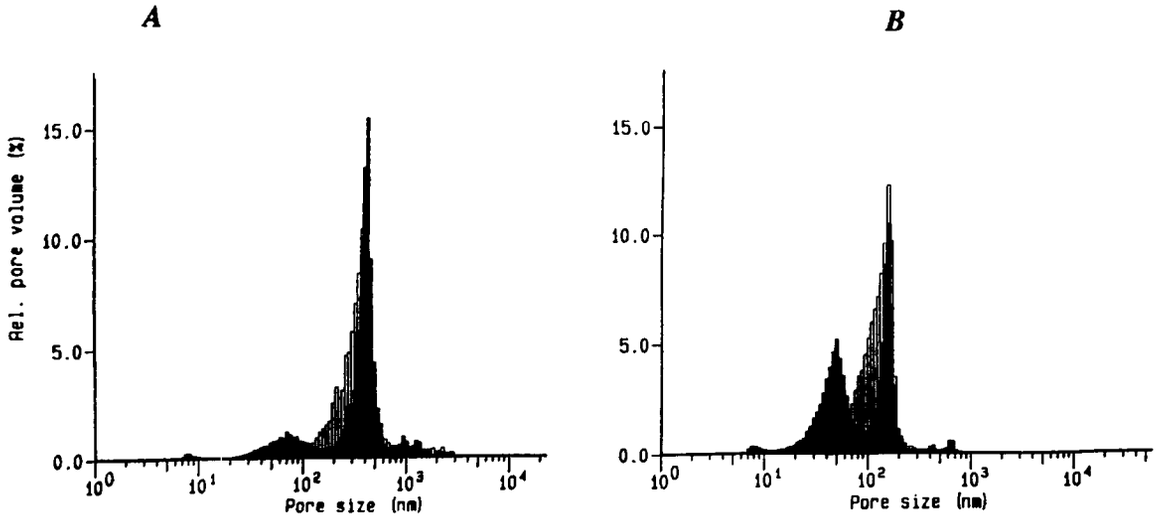

Fig. 8. Pore size distributions of foils with and without binder. A, coarse particle foil made with 6.5 wt.-% PVA 125-98 and 2.6 wt.-% TEG with respect to the ceramic powder (black) and a coarse particle foil released from organic material (white); B, fine particle foil made with 8.0 wt.-% PVA 125-98 and 6.0 wt.-% TEG with respect to the ceramic powder (black) and a fine particle foil released from organic material (white).

Figure 1 is quite helpful for the interpretation of the results of Fig. 7. The large pores (large peak) found in green foils are more or less empty ones and the peak for smaller dimensions are pores partly filled with binder. In the case of no TEG, only large pores exist. This means that some pores are filled completely with binder and others are not filled at all, i.e. there is an inhomogeneous binder distribution. Foils made in the presence of TEG show a more homogeneously distributed binder.

Remarkable is that the peaks of the large pores in the green foils are fairly thin, whereas those found in foils without binder are much broader. Figure 8 compares these two peaks with each other. The peaks of the green foils are drawn in black. It can be seen very clearly that smaller pores are preferentially filled with binder over the larger ones.

In this study, we have used the ratio of the intruded mercury into small pores over that into large pores as a measure of the binder distribution. A larger peak ratio means a more homogeneous binder distribution by this definition. Peak ratios, as a function of TEG concentration in the slip, are given in Fig. 9 for three different types of foil. As can be seen in this figure, the peak ratio increases strongly for larger TEG contents, which indicates a better-distributed binder. The data of the foils presented in Fig. 9 can be more or less described by one single exponential curve.

As already stated in Section 4.2., differences may be found when the same sample is measured for the second time (second run). Figure 10 shows the differences between a first and a second run for both a coarse powder and a fine powder foil. The peak of the small pores is hardly influenced, while the peak of the large ones is quite suppressed in the second run. As a consequence, the peak ratios of the second run are always somewhat larger than those of the first one. This can also be clearly seen in Fig. 9. Both peak ratios determined from the first run and those from the second run are plotted in this figure. The positions of the peaks, however, do not change whether the measurement is carried out the first time or the second time. Not only the height of the peak at small pore dimensions is influenced by the TEG content in the slip but also the position is affected. Figure 11 shows the relative position of the maximum of the peak as a function of the TEG content for different types of foil. The relative position is defined as the pore size at the maximum of the peak divided by the d_{50} pore size of the same foil without binder. The peak maximum of the small pores shifts to larger sizes as the TEG content in the slip becomes higher. Remarkably,

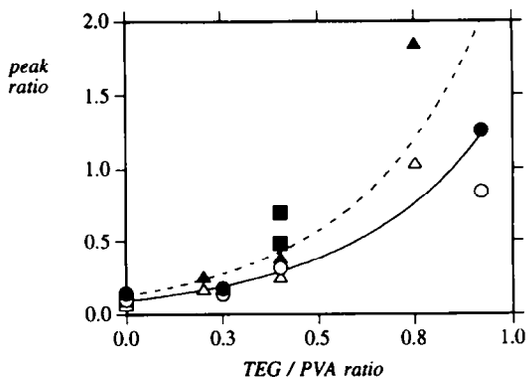

Fig. 9. Peak ratios as a function of the TEG/PVA weight ratio in the slip: circles, coarse particles foils with 6.5 wt.-% PVA 125-98; squares, coarse particle foils with 8.0 wt.-% PVA 125-98; triangles, fine particle foils with 8.0 wt.-% PVA 125-98; open symbols (solid line), data from a first run; filled symbols (dotted line), data from a second run.

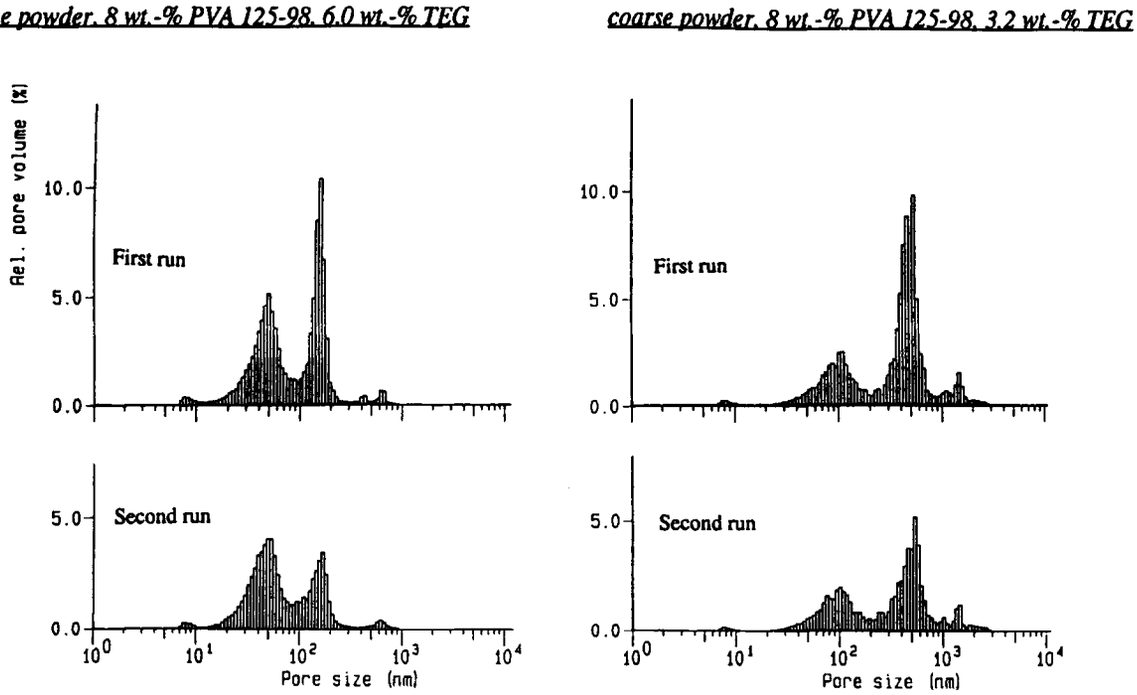

Fig. 10. Pore size distribution differences between a first measuring run and a second one.

the relative positions of these peaks fall on the same curve for both coarse and fine particle foils. Hence, the influence of TEG on the pore sizes in green foils seems to be the same for foils consisting of these two particle sizes.

The B.E.T. results of foils made with different amounts of TEG are given in Fig. 12. The binder distribution index X (see Section 4.1.1) increases with TEG concentration, indicating a more homogeneous binder distribution with increasing TEG content. The X index is negative for low TEG contents, which suggests that small pores are preferentially filled with binder over large ones. The X index reaches a value of unity at a TEG/PVA ratio of about 0·8. Based on the model described in Section 4.1.1, this means a fairly homogeneously distributed binder. The same effect could be seen for the porosity measurement results shown in Fig. 9. The peak ratio increases sharply at TEG/PVA ratios of about 0·8, also indicating a homogeneous binder distribution. Remarkable in Fig. 12 is that the binder distribution index is somewhat lower for the fine particle foils than for coarse particle foils.

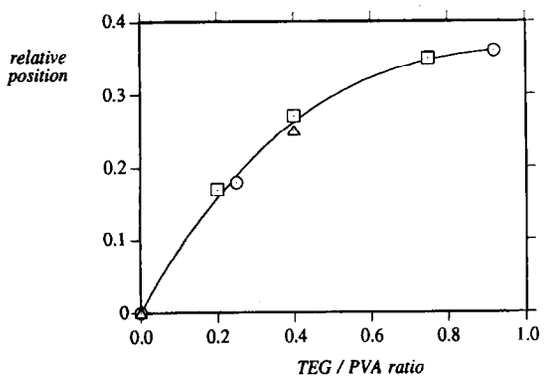

Fig. 11. The relative position of the peak of small pores (i.e. pore size at the maximum of the peak divided by the d_{50} pore size of the same foil without binder) as a function of the TEG/PVA weight ratio: ○, coarse particle foil, 6.5 wt.-% PVA 125-98; Δ, coarse particle foil, 8.0 wt.-% PVA 125-98; □, fine particle foil, 8.0 wt.-% PVA 125-98.

5.2.2.2 PVA type. All the results given above are based on foils made with PVA type 125-98. Do these results also hold for other types of binder? Tables 4 and 5 compare the binder distribution in foils containing either PVA 125-98 or PVA 205-88. Just as in the case of PVA 125-98, foils with PVA 205-88 get a more homogeneous binder distribution when more TEG is used in the slip. The peak ratios from the porosity measurements, as well as the binder distribution indices determined by B.E.T. measurements show,

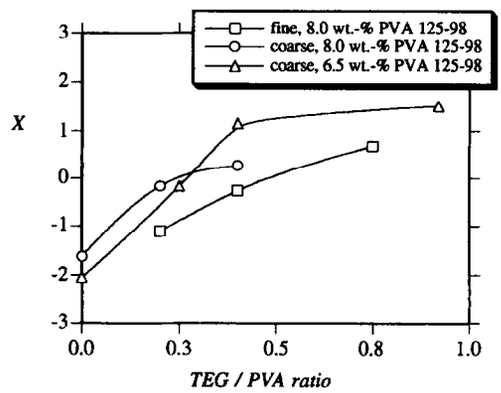

Fig. 12. The binder distribution index as a function of the TEG/PVA weight ratio in the slip.

Table 4. Peak ratios from porosity measurements as a function of the binder type in coarse particle foils

PVA conc. (wt%)	*TEG conc. in the slip (wt%)*	*Peak ratio[a] for PVA 205-88*	*Peak ratio[a] for PVA 125-98*
6·5	0	0·00/0·03	0·10/0·14
6·5	2·6	0·14/0·14	0·31/0·47
8	0	0·06/0·05	0·08/0·10
8	3·2	0·28	0·48/0·70
8 (6·5 + 1·5 PVA 27-98)	3·2	0·25/0·16	0·52

[a]The first number is from a first run, the second is from a second run.

Table 5. The binder distribution index (X) as a function of the binder type in coarse particle foils

PVA con. (wt%)	*TEG conc. in the slip (wt%)*	*X for PVA 205-88*	*X for PVA 125-98*
6·5	0	−2·27	−2·05
6·5	2·6	−1·17	1·15
8	0	−2·16	−1·62
8	3·2	−1·40	0·27
8 (6·5 + 1·5 PVA 27-98)	3·2	−1·42	0·86

however, that at a given TEG concentration in the slip, PVA 205-88 is less homogeneously distributed in foils than PVA 125-98. Even for foils made without TEG, PVA 205-88 is less well distributed. PVA 205-88 differs from PVA 125-98 in two ways, i.e. the molecular weight of PVA 205-88 is higher and the hydrolysis ratio is lower. Which of these properties is responsible for the differences observed? We have plotted the binder distribution index as a function of the relative amount of less-hydrolysed binder in a two-component binder mixture in Fig. 13. As can be seen, the binder distribution index becomes consistently lower for a higher amount of less-hydrolysed PVA types. Hence, most probably, the hydrolysis degree is responsible for the differences found for PVA 125-98 and for PVA 205-88. It is known that some physical properties of PVA (for instance, dissolution behaviour, viscosity, melting point, glass transition temperature) change (drastically) if the hydrolysis ratio reaches 100%.[29]

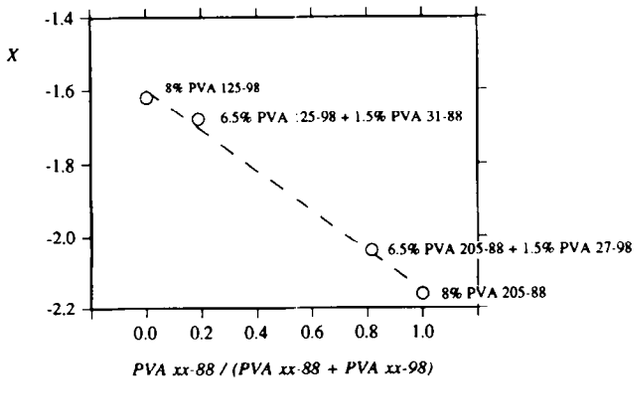

Fig. 13. The binder distribution index as a function of the relative amount of 88% hydrolysed PVA (see Table 1). Foil system: coarse $BaTiO_3$ with 8·0 wt.-% PVA, and no TEG.

5.2.2.3 PVA concentration. The binder distribution index X calculated from the specific surface area of foils is defined in such a way that a comparison between foils containing different amounts of PVA is possible. Table 6 gives X-values for coarse particle foils containing either 6·5, 8·0, 10 or 12 wt% PVA 125-98 with respect to the ceramic material.

The TEG content in the slip is kept constant with respect to the ceramic powder (i.e. 1·6 wt%). This means, however, that the TEG/PVA ratio decreases with increasing amounts of PVA. Hence, a decreasing effect on the binder distribution index may be expected because of a decreasing TEG content with respect to the binder concentration. As can be seen in Table 6, the X-value is negative for the relatively low PVA concentrations and positive for the higher ones. A relatively large difference in binder distribution is found for foils with 8·0 and 10 wt% PVA. To be conclusive, a higher PVA concentration with respect to the ceramic content also leads to a better-distributed binder in the foil.

Table 6. Binder distribution index as a function of binder content in green coarse particle foils; in all cases, the TEG concentration was equal to 1·6 wt% with respect to the ceramics

PVA 125-98 conc. (wt%)	*TEG/PVA (wt/wt)*	*X*
6·5	0·25	−0·17
8·0	0·20	−0·17
10	0·16	0·84
12	0·13	0·57

6 Interpretation/Discussion

In this section, we will try to elucidate the mechanism of how binder is distributed over the foil during drying. Especially, the results obtained for green foils in the previous sections and the drying model as described in Section 2 will be the keys for understanding this mechanism.

Important for the distribution of binder over green foils is the moment in the drying process (i.e. at which part of which drying stage) that the binder gets fixed in the ceramic structure by precipitation, gelation or whatever. Factors that influence this fixation process affect also the binder distribution in foils. Other kinds of factors, such as parameters that influence the accumulation of binder molecules onto ceramic particles due to physical (chemical) interactions, may have also an effect on the binder distribution.

As shown in the previous chapter, several parameters affect the PVA distribution in foils. All of these parameters, however, do not alter the ceramic structure of foils. The porosity of the ceramic structure is even independent of the particle size. The ceramic structure of foils has been built at the end of the constant rate period, i.e. the critical point. This suggests that the binder is not precipitated, gelated or whatever during the constant rate period for the systems analysed in this study. Otherwise, an effect on the ceramic structure of the parameters that influence the fixation process of the binder would have been observed. The supposition that the binder is not yet fixed at the end of the constant rate period is supported by the fact that after complete drying, smaller pores appears to be preferentially filled with binder over the larger ones. This can be explained by the difference in capillary pressures of large and small pores during the first falling rate period. Solution with binder is transferred from large pores to small ones due to this pressure difference. If the totality of the binder had already been fixed in this stage, the binder could not have been transferred in this way. The fact that in some cases binder is observed at the lower side of the foil (the side that has made contact with the carrier) also suggests that the binder is still in solution as the drying process enters the first falling rate period (FRP1). In the FRP1 stage, pores at the upper side of the foil are emptied first and pores that are still filled with solution are enriched with binder by diffusion. This diffusion process is only possible if an amount of the binder is still solved. Hence, for the systems described in this report, the fixation of binder does not notably take place before the critical point is reached.

A very homogeneous binder distribution in green foils will probably be established if the fixation of the binder occurs just at the critical point. In this situation, all pores are still filled with solution with the same binder concentration. The later the point of fixation in the drying process, the less homogeneous is the binder distribution. Binder will then be found more and more in the smaller pores and at the bottom of the foil. This corresponds with very low (negative) X-values.

As shown in the previous section, the binder distribution in foils is influenced by the concentration of TEG and the amount of PVA in the slip. Obviously, the more organic material in the system, the sooner this material is fixed after the critical point in the drying process. However, this certainly does not explain all the results reported in this paper. The binder type also has an influence on the binder distribution. Although not shown in this paper, the drying conditions (external factors) appear to affect the binder distribution in foils as well. Triethylene glycol is known to gelate PVA (one piece of gel may be formed after mixing of PVA and TEG in the appropriate concentrations and waiting for a certain time). With more TEG in the slip, the gelation process will set in earlier, resulting in a more homogeneous binder distribution. PVA types with lower degrees of hydrolysis are somewhat less susceptible to gelation by TEG. These polymers are also better solvable in water than fully hydrolysed ones.[29] Hence, the fixation point is postponed for less-hydrolysed PVA types and, as a consequence, the binder is more heterogeneously distributed.

The external factors for the drying process (air flow, ambient temperature and vapour pressure) can also be expected to have an influence on the fixation process of the binder by TEG. The wet bulb temperature and the speed of drying, which are controlled by these factors, influence the gelation process. Gelation will be set in later when the wet bulb temperature is higher (i.e. a higher ambient temperature and a higher degree of humidity). Most gelation processes are kinetically not very fast. That means that if the drying speed is lowered, the gelation has more time to proceed. Effectively, the gelation point will then be found earlier in the drying process.

The concentration of the binder and that of the plasticizer (provided no plasticizer has been evaporated during drying) at the critical point can be simply calculated using the porosity of foils released from binder, the solid content of the slip and the PVA and TEG concentrations in the slip. The solid content of the system at the critical point can be calculated from the porosity of foils released from binder. The difference in solid content of the slip and that of the system at the critical

point yields the factor with which the concentrations of the organic species have been concentrated at the critical point. In our case, this turns out to be about 5·5. So, the concentrations for gelation at the drying conditions used are probably higher. In principle, an estimate of the gelation concentrations can be made from the peak positions in the pore size distribution diagrams. The volumetric filling percentage of pores with binder can be calculated from the dimensions of an empty pore and those of a filled one. This percentage is then easily transformed into the PVA and TEG concentration at binder fixation, knowing the relative PVA and TEG concentration in the slip. The following uncertainties make this estimate, however, too unreliable:

1. the pore geometry,
2. the way a pore is filled with binder,
3. whether or not TEG has been evaporated before the fixation point is reached during the drying process,
4. the filling degree of pores filled with binder solution when fixation starts,
5. the size of the empty pore (this is not well defined because large pores are emptied firstly during drying).

The peak in the pore size diagram at the small pore size shifts to a larger size when more TEG is used in the slip (see Fig. 11). Two causes may be responsible for this effect:

1. The fixation of the binder starts at a lower PVA concentration in the pores when more TEG is used. After complete drying, less PVA has been left in the individual pores and therefore the open space in pores is larger.
2. When more TEG is used, more TEG will be present in the pores at the fixation point. After removal of TEG from the foil by evaporation or diffusion, more open space will be left.

Another point to remark on is that although a binder distribution may be very inhomogeneous, the *C*-values found were still very close to that of pure PVA. This means that all particles are at least coated with a very thin layer of PVA, even the particles forming empty pores. This may be caused by adsorption of PVA onto the particles. However, the particles are already coated with an adsorption layer of dispersant. Hence, that would mean that PVA adsorbs onto this dispersant layer (displacement is not probable[30]). The effect of a low *C*-value may also be related to the fact that in the first falling rate period, most of the evaporation still occurs at the exterior surface due to continuous thin liquid pathways in pores, along flow is still possible (funicular condition).

We have noticed, that in many cases, the *X*-values for fine particle foils are somewhat smaller than for coarse particle foils, using the same recipe and processing conditions. This may be explained by the differences in capillary pressure that occur within the foil during drying. Pore sizes and the width of the pore distribution are, of course, important in this respect.

7 Conclusions

Both B.E.T. and Mercury Intrusion Porosimetry measurements are useful to characterize the binder distribution in green foils. The results obtained using both techniques are fully in agreement with each other.

Ceramic foils consisting of either a coarse $BaTiO_3$ powder (d_{50} = 0·75 μm) or a fine $BaTiO_3$ powder (d_{50} = 0·20 μm) could be made with the same porosity. The pore sizes in the foils scaled with the particle sizes of the respective powders.

The binder and plasticizer concentrations in the slip used in this study do not change the ceramic structure of foils. Only the binder distribution is influenced by these parameters.

The moment in the drying process of foils that the binder gets fixed in the ceramic structure determines the binder distribution in foils. Factors influencing this fixation process affect the binder distribution. The plasticizer triethylene glycol (TEG) promotes fixation of PVA by a gelation process. More TEG in the slip leads to a more homogeneous binder distribution in foils. In the case of little TEG in the slip, small pores are preferentially filled with binder over large ones and the lower side of foils is enriched with binder. Less-hydrolysed PVA types are less susceptible to gelation with TEG, resulting in a more heterogeneous binder distribution.

All powder particles are covered with PVA molecules, both in foils with a homogeneous binder distribution and in ones with a very heterogeneous binder distribution.

References

1. Ward, P., MLCs — present practices and future trends. In *Ceramic Technology International* 1994, ed. I. Birkby. Sterling Publications Limited, 1994, p. 78.
2. Mistler, R. E., Tape casting: the basic process for meeting the needs of the electronic industry. *Ceram. Bull.*, **69** (1990) 1022–6.
3. Cronin, D. J. & McMarlin, K. A., Tape casting of dielectric substrates. In *Ceramics Today — Tomorrows's Ceramics*, ed. P. Vincenzini. Elsevier Science Publishers B.V., 1991, pp 1963–72.
4. Fransen, B. C. H., Janssen, G. J., Oostra, S. J. J. & de Vries J. W. C., Integration of mechanics and electronics:

low voltage ceramic multilayer actuators. In *6th Capacitor and Resistor Technology Symposium CARTS, '92*, Brugge, 1992, pp. 128–33.
5. Phillips, S. V. & Datta, A. K., Ceramic tape casting for Oxide Fuel Cell (SOFC) electrolyte production. In *Proc. Ceramics in Energy Applications*, Sheffield, 1990, p. 183.
6. Heinrich, J., Huber, J., Förster, S. & Quell, P., Advanced ceramics as heat exchangers in domestic and industrial appliances. *Industrial Ceram.*, **7** (1987) 34.
7. Phillips, S. V., Howard, P. J., Partridge, G. & Datta, A. K., Fabrication routes for superconducting ceramics. *British Ceramic Proceedings No. 40, Superconducting Ceramics*, 1988, p. 31–6.
8. Boch, P., Chartier, T. & Huttepain, M., Tape casting of Al_2O_3/ZrO_2 laminated composites. *J. Am. Ceram. Soc.*, **69** (1986) C-191-2.
9. van der Sanden, M. C. M., Ultimate toughness of amorphous polymers. Thesis, University of Technology Eindhoven, 1993.
10. Cima, M. J., Lewis, J. A. & Devos, A. D., Binder distribution in ceramic greenware during thermolysis. *J. Am. Ceram. Soc.*, **72** (1989) 1192–9.
11. de With, G., Structural integrity of ceramic multilayer capacitor materials and ceramic multilayer capacitors. *J. Eur. Ceram. Soc.*, **12** (1993) 323–36.
12. Bortzmeyer, D., Langguth, G. & Orange, G., Fracture mechanics of green products. *J. Eur. Ceram. Soc.*, **11** (1993) 9–16.
13. Hennings, D. F. K., Schreinemacher, B. & Schreinemacher, H., High-permittivity ceramics with high endurance. *J. Eur. Ceram. Soc.*, **13** (1994) 81–8.
14. Hennings, D., Barium titanate based ceramic materials for dielectric use. *Int. J. High Tech. Ceram.*, **3** (1987) 91–111.
15. Bergholz, A. & Ferber, C., Bedeutung der Strömungstechnik für die Trocknung keramischer Produkte. *Keram. Z.*, **44** (1992) 88–92.
16. Streicher, E. & Chartier, T., Study of cracking and microstructural evolution during drying of tape-cast aluminium nitride sheet. *J. Mater. Sci.*, **26** (1991) 1659–65.
17. Scherer, G. W., Theory of drying. *J. Am. Ceram. Soc.*, **73** (1990) 3–14.
18. Chen, Z.-C., Powder processing of barium titanate ceramics with polyacrylic acid. Thesis, University of Lausanne, 1992.
19. Simpkins, P. G., Johnson, D. W. & Fleming, D. A. Jr., Drying behaviour of colloidal silica gels. *J. Am. Ceram. Soc.*, **72** (1989) 1816–21.
20. Zhang, Y., Tang, X. & Uchida, N., Mathematical simulation for segregation of PVA during drying. *J. Ceram. Soc. Jpn, Int. Edn*, **101** (1993) 177–80.
21. Chiu, R. C. & Cima, M. J., Drying behaviour of granular ceramic films. *Ceram. Trans. (Ceramic Powder Science IV)*, **22** (1991) 347–56.
22. Chartier, T., Tape casting. In *Encyclopedia of Advanced Materials*, ed. D. Bloor, R. J. Brook, M. C. Flemings & S. Mahajan. Pergamon Press, 1994, pp. 2763–7.
23. Spauszus, S. & Rauscher, H.-U., Formgebungs Prinzipien und Arbeitsgrenzen bei der Herstellung dünner Keramikfolien. *Keram. Z.*, **44** (1992) 23–7.
24. Chartier, T. & Bruneau, A., Aqueous tape casting of alumina substrates. *J. Eur. Ceram. Soc.*, **12** (1993) 243–7.
25. van Brakel, J., Modry, S. & Svatá, M., Mercury porosimetry: state of the art. *Powder Technol.*, **29** (1981) 1–12.
26. Whittemore, O. J., Mercury porosimetry of ceramics. *Powder Technol.*, **29** (1981) 167–75.
27. Moscou, L. & Lub, S., Practical use of mercury porosimetry in the study of porous solids. *Powder Technol.*, **29** (1981) 45–52.
28. Opitz, J. & Gontermann-Gehl, U., Porenstruktur dünner keramischer Folien. *Sprechsaal*, **125** (1992) 682–7.
29. Finch, C. A. (ed.), *Polyvinyl Alcohol Developments*. John Wiley & Sons, New York, 1992.
30. van der Beek, G. P., Displacement of adsorbed polymers. A systematic study of segment-surface interactions. Thesis, Agricultural University of Wageningen, 1991.

Appendix: Relationships between the surface area and the binder distribution in foils (eqns (1)–(4))

A1 Spherical pores filled homogeneously with binder

Suppose a porous system has N equal spherical pores of radius R. The empty porous system has a surface area A_0 and a volume V_0 which are given by

$$A_0 = 4\pi R^2 N \tag{A1}$$

$$V_0 = \frac{4}{3}\pi R^3 N \tag{A2}$$

Filling the porous system proceeds in such a way that the radii of all pores decrease equally. The surface area of a system filled with a certain amount of binder is then equal to

$$A = 4\pi r^2 N \quad \text{with } 0 \le r \le R \tag{A3}$$

The volume of added material, V_a, can be expressed in the following way

$$V_a = \frac{4}{3}\pi(R^3 - r^3)N \quad \text{with } 0 \le r \le R \tag{A4}$$

Combining relations (A1)–(A4) yields eqn (A5)

$$A = A_0 \left[1 - \frac{V_a}{V_0}\right]^{2/3} \tag{A5}$$

The volume of the empty porous system, V_0, can also be expressed in terms of the porosity P_0 and the total volume V_{tot} of the system without additions

$$V_0 = \frac{P_0}{100} V_{tot} \tag{A6}$$

In the same way, the volume of the ceramic material is given by

$$V_{cer} = \frac{(100 - P_0)}{100} V_{tot} \tag{A7}$$

A definition of the amount of added organic substances (V_i), expressed in vol.% with respect to the ceramic material, is given in eqn (A8)

$$V_i = \frac{V_a}{V_{cer}} 100 \tag{A8}$$

The factor V_a/V_0 in eqn (A5) can be expressed in the following way, using eqns (A6)–(A8)

$$\frac{V_a}{V_0} = \frac{(1 - P_0/100)}{P_0} V_i \tag{A9}$$

Because the maximum value for the ratio V_a/V_0 is 1, V_i can by definition not be larger than $P_0/(1 - P_0/100)$.

Substitution of the last equation into (A5) yields the following formula, which is identical to eqn (1):

$$A = A_0 \left[1 - \frac{1-P_0/100}{P_0} V_i\right]^{2/3} \quad \text{(A10)}$$

Usually, the concentrations of organic substances in slips and foils are given in wt% with respect to the solid content. The parameter V_i can easily be calculated from the concentrations defined in this way using eqn (A11)

$$V_i = C_i \frac{\rho_{cer}}{\rho_i} \quad \text{(A11)}$$

with ρ_i the specific density of substance i, C_i the concentration of substance i in wt% with respect to the ceramics and ρ_{cer} the density of the ceramic material.

A2 Pores filled inhomogeneously with binder

In this case, filling of the porous system proceeds by lowering the number of empty pores. Pores are completely filled one by one. The number of filled pores is equal to n. The surface area and the volume of one pore are a_0 and v_0, respectively. Relations (A12)–(A15) are of the same kind as eqns (A1)–(A4).

$$A_0 = a_0 N \quad \text{(A12)}$$

$$V_0 = v_0 N \quad \text{(A13)}$$

$$A = a_0(N-n) \quad \text{with } 0 \le n \le N \quad \text{(A14)}$$

$$V_a = v_0 n \quad \text{with } 0 \le n \le N \quad \text{(A15)}$$

Combining the last four equations gives

$$A = A_0 \left[1 - \frac{V_a}{V_0}\right] \quad \text{(A16)}$$

The link between eqns (A16) and (A17) is the same as in the previous case, and

$$A = A_0 \left[1 - \frac{1-P_0/100}{P_0} V_i\right] \quad \text{(A17)}$$

Because we did not assume any pore geometry for the derivation of eqn (A17), this dependency is invariant for the pore geometry!

A3 Cylindrical pores filled homogeneously with binder

In this case, the porous system is modelled as a body containing N cylindrical pores of length z. Addition of organic material reduces the diameter of all cylinders, i.e. this is a homogeneous filling. The same kind of formulas are derived as in the previous cases

$$A_0 = 2\pi R z N \quad \text{(A18)}$$

$$V_0 = \pi R^2 z N \quad \text{(A19)}$$

$$A = 2\pi r z N \quad \text{with } 0 \le r \le R \quad \text{(A20)}$$

$$V_a = \pi(R^2 - r^2) z N \quad \text{with } 0 \le r \le R \quad \text{(A21)}$$

These equations lead to

$$A = A_0 \left[1 - \frac{V_a}{V_0}\right]^{1/2} \quad \text{(A22)}$$

and

$$A = A_0 \left[1 - \frac{1-P_0/100}{P_0} V_i\right]^{1/2} \quad \text{(A23)}$$

A4 Small spherical pores are preferentially filled with binder over large ones

In the previous cases, we have modelled the porous structure as a body containing a number of equally sized pores. Equations (A10), (A17) and (A23) also hold for ceramic structures containing different pore sizes, but the added organic material must then be distributed equally over the size distribution. In this instance, the added organic material is not distributed equally over the size distribution. We assume three different spherical pores with radii $0{\cdot}5R$, R and $2R$. These pore types are denoted in the following relations with one prime, two primes and three primes, respectively. The number of each type of pore is chosen such that the volume of each class of pores is equal to 1/3 of the total volume of pores. Hence,

$$V'_0 = \frac{1}{3} V_0 = \frac{4}{3}\pi (0{\cdot}5R)^3 \frac{64N}{73} \quad \text{(A24)}$$

$$V''_0 = \frac{1}{3} V_0 = \frac{4}{3}\pi R^3 \frac{8N}{73} \quad \text{(A25)}$$

$$V'''_0 = \frac{1}{3} V_0 = \frac{4}{3}\pi (2R)^3 \frac{N}{73} \quad \text{(A26)}$$

The surface area of each class of pore without organic material is given by the following three formulas

$$A'_0 = a'_0 \frac{64N}{73} = \frac{4}{7} A_0 \quad \text{(A27)}$$

$$A''_0 = a''_0 \frac{8N}{73} = \frac{2}{7} A_0 \quad \text{(A28)}$$

$$A'''_0 = a'''_0 \frac{N}{73} = \frac{1}{7} A_0 \quad \text{(A29)}$$

Now added material is not the distributed equally over pores of different sizes. Firstly the small pores are filled, then the medium sized ones and finally the pores with the largest radii. Filling of the porous system proceeds in such a way that the number of pores decreases with the added amount (i.e. inhomogeneous distribution). The surface area A and the added amount of material V_a as a function of the number of occupied pores n are given by the follows equations:

$$\begin{cases} A = A_0 - a'_0 n \\ V_a = v'_0 n \end{cases} \quad \text{for } 0 \le n \le \frac{64N}{73} \tag{A30}$$

$$\begin{cases} A = \frac{3}{7} A_0 - a''_0 (n - \frac{64N}{73}) \\ V_a = \frac{1}{3} V_0 + v''_0 (n - \frac{64N}{73}) \end{cases} \quad \text{for } \frac{64N}{73} \le n \le \frac{72N}{73} \tag{A31}$$

$$\begin{cases} A = \frac{1}{7} A_0 - a'''_0 (n - \frac{72N}{73}) \\ V_a = \frac{2}{3} V_0 + v'''_0 (n - \frac{72N}{73}) \end{cases} \quad \text{for } \frac{72N}{73} \le n \le N \tag{A32}$$

In the same way as in the previous cases, these equations lead to

$$A = A_0 \left[1 - \frac{12}{7} \left(\frac{1-P_0/100}{P_0}\right) V_i\right] \quad \text{for } 0 \le V_i \le \frac{1}{3} \frac{100P_0}{(100-P_0)} \tag{A33}$$

$$A = A_0 \left[\frac{5}{7} - \frac{6}{7} \left(\frac{1-P_0/100}{P_0}\right) V_i\right] \quad \text{for } \frac{1}{3} \frac{100P_0}{(100-P_0)} \le V_i \le \frac{2}{3} \frac{100P_0}{(100-P_0)} \tag{A34}$$

$$A = A_0 \left[\frac{3}{7} - \frac{3}{7} \left(\frac{1-P_0/100}{P_0}\right) V_i\right] \quad \text{for } \frac{2}{3} \frac{100P_0}{(100-P_0)} \le V_i \le \frac{100P_0}{(100-P_0)} \tag{A35}$$